TRANSITION IN THE MINIMUM IGNITION ENERGY FOR THE LOCALISED FORCED IGNITION OF TURBULENT HOMOGENEOUS MIXTURES

C. Turquand d'Auzay[1], *V. Papapostolou*[1], *S.F. Ahmed* [2] *and N. Chakraborty*[1]

[1] *School of Engineering, Newcastle University, Newcastle Upon-Tyne, NE1 7RU, UK*
[2] *Department of Mechanical and Industrial Engineering, College of Engineering Qatar University, P. O. Box 2713, Doha, Qatar*

nct92@ncl.ac.uk

Abstract

Localised forced ignition of turbulent homogeneous mixtures plays a significant role in the design of efficient and reliable engines. The Minimum Ignition Energy (MIE) needed to obtain a self-sustained propagation of the ignition kernel has been experimentally investigated. A transition in the rate of increase of MIE with increasing root-mean-square turbulent velocity fluctuation between low and high turbulence intensities has been found experimentally, and has yet to be numerically analysed. Multiple three-dimensional Direct Numerical Simulations have been performed under homogeneous isotropic decaying turbulence at several initial turbulence intensities. A transition in the MIE has been found and appears qualitatively consistent with the experimental results. The highly stochastic behaviour of the ignition mechanism is also well reproduced. The balance of energy following its deposition is investigated to highlight the physical mechanisms leading to the success or failure of the ignition event. Finally, it was found that the spatial curvature fluctuations affect the normal component of thermal diffusion. This, in turns, affects the overall diffusion term which plays a key role in the ignition success.

1 Introduction

Localised forced ignition (e.g. laser, spark) of homogeneous mixture plays an important role in safety standards as well as in the design of efficient and reliable Spark ignition and Direct Injection engines, in which misfire causes ineffective combustion. Because of its fundamental importance, the localised forced ignition has been extensively studied by numerous researchers by analytical (Espi and Liñán, 2001), experimental (Bradley, 1987 ; Ballal and Lefebvre, 1975 ; Huang *et al.*, 2007 ; Shy *et al.*, 2010) and numerical (Baum and Poinsot, 1995 ; Klein *et al.*, 2008 ; Patel and Chakraborty, 2015) means. The analytical analysis, although conducted for laminar quiescent flows, provided fundamental insights into the localised forced ignition and a satisfactory agreement with the experimental findings was found. An extensive analysis of the influence of the equivalence ratio and turbulence intensity on the critical radius for successful spark ignition was carried out (Ballal and Lefebvre, 1975). It was found that the minimum energy requirement for successful ignition increases with turbulence intensity and departure from stoichiometry.

Shy and co-workers (Huang *et al.*, 2007, Shy *et al.*, 2010) further concentrated on the minimum ignition energy (MIE, minimum energy deposited in the flow to obtain a successful ignition of the mixture and subsequent flame propagation) under homogeneous isotropic turbulence and for different equivalence ratios of homogeneous methane-air mixtures. Due to the detrimental effects of turbulence, the MIE was found to increase with increasing u'/s_l^0 (where u' is the root-mean-square velocity fluctuation and s_l^0 is the unstrained laminar stoichiometric burning velocity). A transition in the MIE is observed at a critical value $(u'/s_l^0)_c$ such that the increase in MIE with increasing u'/s_l^0 is significantly higher for $u'/s_l^0 \geqslant (u'/s_l^0)_c$ than for $u'/s_l^0 \leqslant (u'/s_l^0)_c$. Scaling arguments presented by Shy *et al.* (2010) justify these findings. The detrimental effects of turbulence on the energy requirement for successful ignition was also demonstrated by Mulla *et al.* (2010) which is consistent with previous findings by Ballal and Lefebvre (1975), Klein *et al.* (2008), Patel and Chakraborty (2015).

In recent times, Direct Numerical Simulation (DNS) has become an important tool for the fundamental understanding and modelling of complex combustion phenomena. It has become possible to carry out DNS of localised forced ignition of homogeneous mixtures to analyse the early stages of the flame development. Patel and Chakraborty (2015) analysed the effects of the characteristic width and duration of energy deposition profile, ignition energy and turbulence intensity for different equivalence ratio values and confirmed the analytical and experimental findings. Inter-

ested readers are referred to Mastorakos (2009) for further details on localised forced ignition. Although the existing numerical investigations (Baum and Poinsot, 1995 ; Patel and Chakraborty, 2015) provide significant physical insights into the localised forced ignition of homogeneous mixtures, the transition of MIE between small and high values of u'/s_l^0 reported experimentally by Shy and co-workers (Huang *et al.*, 2007 ; Shy *et al.*, 2010) has not yet been computationally analysed. This work thus aims at addressing this deficit in the existing literature.

In the present analysis, the MIE has been evaluated across a range of turbulence intensities using three-dimensional single-step chemistry DNS under decaying homogeneous isotropic turbulence. The energy deposition emulates a localised forced ignition by depositing a fixed amount of energy at a given location for a specified period of time. The initial flow conditions are chosen such that the combustion situations span from the wrinkled flamelets to the thin reaction zones regimes of premixed combustion. The simulations have been used to determine the MIE which leads to either a successful ignition but not necessarily to a self-sustained combustion or to a successful self-propagating flame once the energy source is switched off. The main objectives of this work are thus (i) to numerically analyse the MIE variation with increasing turbulence intensity and (ii) to provide physical explanations for the success or failure of the ignition event.

2 Mathematical formulation

The simulations have been carried out using the three-dimensional compressible DNS code SENGA (Patel and Chakraborty, 2015), in which the conservation equations of mass, momentum, energy and mass fractions are solved on a Cartesian grid with uniform grid spacing. The code employs high-order finite-difference (10^{th}-order for internal points and decreasing to 2^{nd}-order at the non-periodic boundaries) and low-storage Runge-Kutta (3^{rd}-order explicit) schemes for spatial and temporal differentiation respectively. The non-periodic boundary conditions are specified using the Navier-Stokes Characteristic Boundary Conditions (NSCBC) technique.

The heat addition by the ignitor for the localised forced ignition is accounted for by the addition of the source term q''' in the energy equation, which reads,

$$\underbrace{\frac{\partial}{\partial t}\rho E}_{} \underbrace{+\frac{\partial}{\partial x_i}\rho u_i E}_{-C_1} = \underbrace{-\frac{\partial}{\partial x_i}u_i P}_{P_1} \underbrace{+\frac{\partial}{\partial x_i}\tau_{ij}u_j}_{D_1} \underbrace{+\dot{\omega}_T}_{P_2}$$
$$\underbrace{+\frac{\partial}{\partial x_k}\left[\lambda\frac{\partial \hat{T}}{\partial x_i}\right]}_{D_2} \underbrace{-\frac{\partial}{\partial x_i}\rho\sum_{k=1}^{N}h_{s,k}Y_k V_{k,i}}_{D_3} \underbrace{+q'''}_{P_3}, \quad (1)$$

where E is the specific stagnation internal energy ($E = C_v\hat{T} + u_i u_i/2$, where C_v is the heat capacity at constant volume), u_i is the i-th velocity component, $h_{s,k}$ is the specific enthalpy, P is the pressure, τ_{ij} is the viscous shear stress and $\hat{T}$ is the dimensional temperature. Note that the species heat capacities as well as the viscosity (μ), the thermal conductivity (λ) and the density-weighted mass diffusivity (ρD) are constant and the same for all species, thus $D_3 = 0$. The source term q''' follows a Gaussian distribution in the radial direction from the ignition point and is expressed as $q'''(r) = A_q \exp(-r^2/R_{sp}^2)$ (Espi and Liñán, 2001), where r is the distance from the ignition centre and R_{sp} is the characteristic width of the energy deposition. The constant A_q is determined using $\dot{Q} = \int_V q'''\,\mathrm{d}V$ where $\dot{Q} = (4/3)a_{sp}\rho_0 C_p \tau T_0 \delta_z^3[H(t) - H(t-t_{sp})]/t_{sp}$, where a_{sp} determines the total energy input, $\tau = (T_{ad}-T_0)/T_0$ is the heat release (where T_0 and T_{ad} are the reactants and adiabatic stoichiometric flame temperatures respectively), δ_z is the Zel'dovich flame thickness ($\delta_z = \alpha_T/s_l^0$, where α_T is the reactant thermal diffusivity) and $H(t)$ is an Heaviside function that ensures that the spark is only active until $t = t_{sp}$. The deposition duration t_{sp} is determined as a function of the chemical time scale such that $t_{sp} = b_{sp}t_l$ where $t_l = \delta_z/s_l^0$. The details of the spark formation (plasma formation, shock wave, etc.) are not considered.

A single-step chemical mechanism has been considered (Fuel + sOxidiser $\rightarrow$ Products where s indicates the mass of oxidiser consumed by unit mass of fuel under stoichiometric conditions) where the fuel reaction rate ($\dot{\omega}_f$) is given by an Arrhenius type expression (Patel and Chakraborty, 2015).

3 Numerical implementation

The computational domain is cubic with a size of $55\delta_z \times 55\delta_z \times 55\delta_z$ such that 6.5 integral eddies are retained in the domain. It is discretised with a grid of $512 \times 512 \times 512$ cells which ensures 10 points across the thermal flame thickness $\delta_{th} = (T_{ad} - T_0)/\max(|\nabla T|_l)$, but also that $\eta > \Delta x$ where η is the Kolmogorov length scale.

In this work, the flame-turbulence interaction occurs in decaying isotropic homogeneous turbulence initially generated using Rogallo's pseudo-spectral method with prescribed initial velocity fluctuations (u') and integral length scale (l_t) obeying the Batchelor-Towsend spectrum (Batchelor and Towsend, 1948). The integral length scale is kept constant at $l_t/\delta_z = 9$, while the initial turbulence intensities varies such that the cases studied span from the laminar to the thin reaction zone regimes as shown on the Peters regime diagram (Peters, 2000) in Fig. 1.

Here, the mixture is representative of a stoichiometric methane/air mixture with $s = 4$, which, with an oxygen mass fraction in pure air of $Y_{o,\infty} = 0.233$, yields a fuel mass fraction of $Y_{f,st} = 0.055$. A progress variable is defined as $c = (Y_{f,st} - Y_f)/Y_{f,st}$ such that it varies monotonically between 0 in the

reactants to 1 in the products. The mixture is preheated to yield $\tau = 3$, and the Zel'dovich parameter is $\beta = 6$ which is representative of methane/air combustion. Standard values have been chosen for the Prandtl number (Pr $= 0.7$) and ratio of specific heat ($\gamma = 1.4$). A constant unity Lewis number is used for all species.

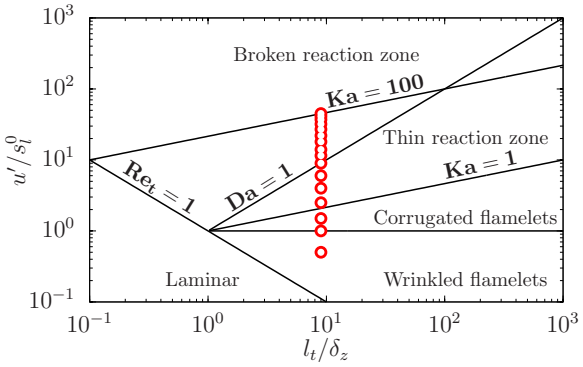

Figure 1: Cases investigated for the MIE transition

The spark's characteristic width and duration are constant throughout the whole study with $R_{sp}/\delta_z = 2.45$ and $b_{sp} = 0.2$ (Patel and Chakraborty, 2015). The spark power a_{sp} is modified until the minimum values sufficient to (i) produce a successful ignition ($T > 1$, where $T = (\hat{T} - T_0)/(T_{ad} - T_0)$ is the non-dimensional temperature) but not necessarily self-sustained combustion and (ii) ensure the self-sustainability of the combustion once the ignitor is switched off ($T > 1$ and burned gas volume increasing with time) are found. To this end, the simulations are run for $t = 3t_{sp}$ for the evaluation of the MIE sufficient for ignition, and up to $t = 10t_{sp}$ for the MIE sufficient for self-sustained flame propagation.

4 Results

MIE transition

Figure 2 shows the variation of normalised MIE ($\Gamma = \text{IE}/\text{MIE}_l^0$, where IE is the input energy and MIE_l^0 is the laminar MIE) for both ignition and self-sustained flame propagation events as a function of the turbulence intensity. For low turbulence intensities, i.e. $u'/s_l^0 \leqslant 6$, Γ_{MIE} is identical for both ignition and propagation, meaning that turbulence effects are weak enough not to influence the flame propagation significantly. At larger u'/s_l^0, the energy needed to obtain a successful ignition and the subsequent flame propagation becomes significantly larger than the one needed for successful ignition alone. This is explained by the fact that the initial kernel needs to reach a radius that is larger than a critical value for the flame to propagate (Ballal and Lefebvre, 1975), and this critical dimension increases with u'/s_l^0. Moreover, Fig. 2 suggests that successful ignition does not necessarily ensure self-sustained flame propagation and the minimum energy requirement to ensure self-sustained flame propagation could be considerably greater than the value which is just about sufficient to ignite the mixture.

In both cases, two different regimes can be observed with a slow increase of the MIE for ignition/propagation with turbulence intensity for small values of u'/s_l^0 and a large increase as the turbulence intensity increases. This behaviour is qualitatively consistent with the experimental data of Shy *et al.* (2010). The critical turbulence intensity at which the transition of the MIE is observed is approximately $(u'/s_l^0)_c \approx 14$ for ensuring just ignition and decreases slightly to $(u'/s_l^0)_c \approx 11.5$ for ensuring self-sustained flame propagation following successful ignition. This is also in good agreement with the experimental results of Shy *et al.* (2010) that obtained $(u'/s_l^0)_c \approx 15$ for a stoichiometric methane/air mixture. The critical Karlovitz number (Ka $= (l_t/\delta_z)^{-1/2}(u'/s_l^0)^{3/2}$) is thus Ka$_c \approx 17$ just for successful ignition and Ka$_c \approx 13$ for successful self-sustained flame propagation following successful ignition, while Shy *et al.* (2010) obtained experimentally Ka$_c \approx 8$ for a similar configuration. In the case of MIE of self-sustained flame propagation following successful ignition, the MIE in the two regimes can be approximated by $\Gamma_{\text{MIE}} \propto (u'/s_l^0)^n$ with $n = 0.03$ for $u'/s_l^0 \leqslant (u'/s_l^0)_c$ and $n = 2$ for $u'/s_l^0 \geqslant (u'/s_l^0)_c$ whereas if was found experimentally by Shy *et al.* (2010) that n varies from 1 for $u'/s_l^0 \leqslant (u'/s_l^0)_c$ to $n = 7 - 16$ for $u'/s_l^0 \geqslant (u'/s_l^0)_c$ for methane-air mixtures.

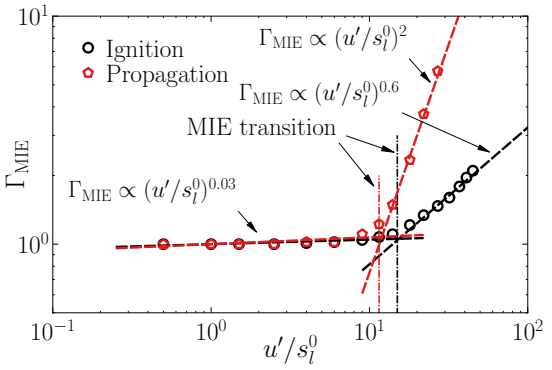

Figure 2: Normalised MIE (Γ_{MIE}) as a function of u'/s_l^0

The quantitative disagreement between the experiment and the DNS can be explained by the fact that the measured energies between these two approaches are not the same. In experiments, the energy transferred from the electrodes to the fluid is not precisely known and varies based on the electrodes material, size, geometry, gap width but also depends on the duration, profile and total energy of the discharge, to which heat losses due to the forced convection with the surrounding fluid must be added. From the energy transferred to the fluid, some is further lost due to plasma formation and the creation of an initial shock wave. Thus the amount of energy that is finally converted to a temperature increase of the fluid is much lower and non-linearly related to the total energy measured at the electrodes. This differs from the DNS in which all the energy added to the flow is converted into a temperature increase.

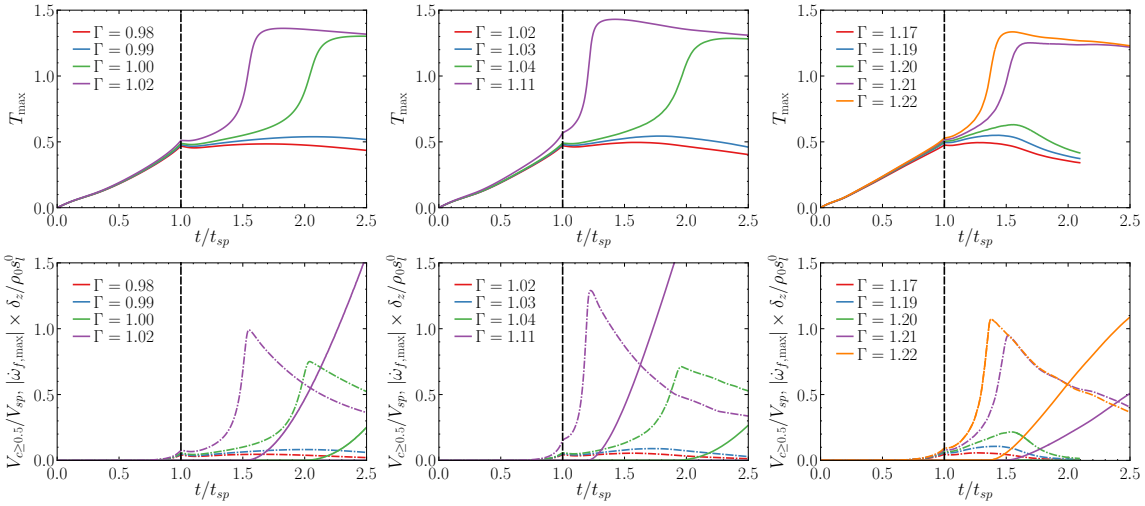

Figure 3: Ignition temporal evolution of **(top)** $T_{\max}$ and **(bottom)** (——) $V_{c\geqslant 0.5}/V_{sp}$ and (- - - -) $|\dot{\omega}_{f,\max}| \times \delta_z/\rho_0 s_l^0$ with from *(left)* to *(right)*, $u'/s_l^0 = 0,\ 9.0,\ 18.0$

Temporal evolutions

The temporal variation of the maximum value of non-dimensional temperature ($T_{\max}$), maximum reaction rate and of the volume defined by $c \geqslant 0.5$ normalised by the spark volume ($V_{sp} = 4/3\pi R_{sp}^3$) are shown in Fig. 3 for different turbulence intensities and energies close to the MIE.

The behaviour observed here matches previous numerical results (Baum and Poinsot, 1995 ; Patel and Chakraborty, 2015), with a maximum temperature increasing continuously during the energy deposition up to $T_{\max} \approx 0.5$ for all values of u'/s_l^0. At $t = t_{sp}$, chemical reactions are only starting as indicated by the low values of $|\dot{\omega}_{f,\max}| \times \delta_z/\rho_0 s_l^0$ and the large thermal gradient created by the energy deposition give rise to a large energy transfer that heats the surrounding unburned mixture. A competition between the temperature diffusion and the heat release by the chemical reaction takes place and leads to a stabilisation of $T_{\max}$. Later on, at $t/t_{sp} \geqslant 1.1$, if the heat release is strong enough, $T_{\max}$ increases again until a thermal runaway occurs when the temperature reaches a value close to $T_c = 1 - 1/\beta$. The non-dimensional temperature T then reaches a maximum larger than unity and the ignition is successful. Simultaneously, the reaction rate varies rapidly in time to reach a maximum and then slowly decreases as $T_{\max}$ decreases.

It is worth mentioning that all ignitions visible in Fig. 3 can be considered as auto-ignition events as the maximum temperature is only reached long after the spark has been switched off. At $t = t_{sp}$, the volume of products is still zero and only starts to increase after the thermal runaway, further strengthening the fact that it is an auto-ignition.

Stochastic behaviour

The ignition success is extremely sensitive to the energy deposited in the mixture, as shown in Fig. 3 at all u'/s_l^0 where an increase by 1% of Γ is enough to obtain a thermal runaway. To investigate the influence of the turbulence on this fundamentally stochastic process, the ignition success rate is measured by sparking two additional initial turbulent fields with identical turbulent (u'/s_l^0, l_t) and sparking (Γ, b_{sp}, R_{sp}) properties. The success rate is reported in Fig. 4, where it can be seen that for low turbulence intensities ($u'/s_l^0 \leqslant 1.5$), different realisations of turbulence do not significantly influence the ignition probability.

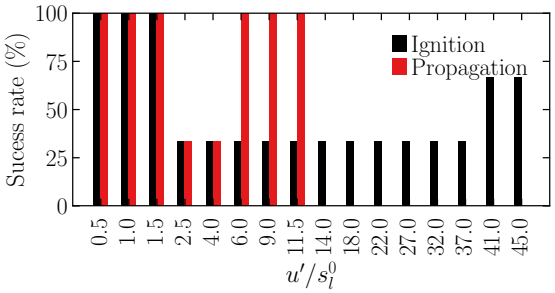

Figure 4: Success rate of ignition and propagation at different turbulence intensities

However, as u'/s_l^0 increases, failed ignition and failed sustained propagation are obtained for some realisations of the statistically identical turbulent flow fields, and this behaviour persists until the very large turbulence intensities ($u'/s_l^0 \leqslant 41$). For these large values of u'/s_l^0, the eddy turnover time t_e ($t_e = l_t/u'$) becomes comparable to the spark time, i.e. $t_e/t_{sp} \approx 1$ which allows some volume of fluid to receive energy multiple times due to the turbulent motion that brings it back within the spark. The probability of propagation is not 100% only at $u'/s_l^0 = 2.5$ and $u'/s_l^0 = 4$ where Γ_{MIE} is identical for both ignition and propagation, which means that the failed propagation is actually here a failed ignition.

Figure 5 shows the temporal evolution of $T_{\max}$ for the different turbulent realisations at several u'/s_l^0. For $u'/s_l^0 = 1$, the temperature profiles appear very similar with an almost identical temperature at $t = t_{sp}$, but a slight time lag ($\Delta t \approx 0.1 t_{sp}$) in reaching the adiabatic temperature can be observed. This is attributed

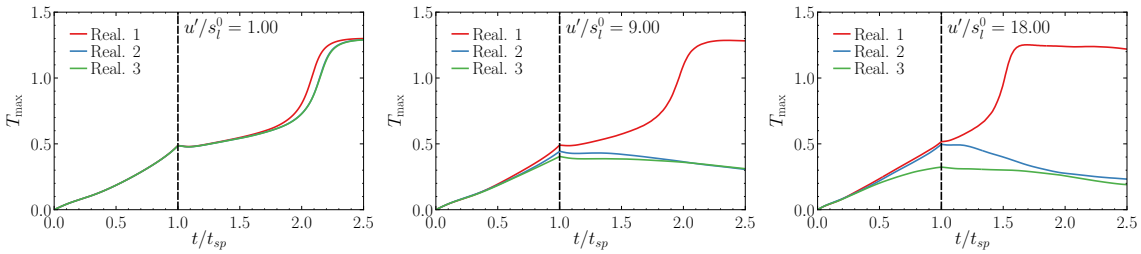

Figure 5: Temporal evolution of $T_{\max}$ for three different realisations of the initial turbulence and $\Gamma = \Gamma_{\text{MIE}}$

to the turbulent motion that slightly alters the way temperature is distributed at $t = t_{sp}$ or $t/t_e \approx 0.02$. For larger turbulence intensities, the ratio t_e/t_{sp} decreases, and turbulent motions become more pronounced during the energy deposition, and thus are able to significantly decrease the maximum temperature reached by increasing the local diffusion.

Energy budget

An accurate understanding of the underlying mechanisms governing the ignition can be gained by analysing the energy balance. The temporal evolution of the energy equation budget (Eq. 1) is presented in Fig. 6 for $u'/s_l^0 = 9$ and $\Gamma = \Gamma_{\text{MIE}}$ for the three different turbulence realisations. Note that qualitatively similar results are obtained for the other values of u'/s_l^0 studied in this work.

For $t/t_{sp} \leqslant 1$, P_3 is non-zero and maximum for high values of T which are found at the ignitor centre. The viscous term (D_1) is not a leading order term and does not play any significant role in the ignition dynamic. The convective (C_1) and pressure work (P_1) terms are linked through the dilatation of gas and follow similar trends.

The last two terms are the energy diffusion (thermal diffusion) (D_2) and the heat release due to the chemical reactions (P_2) respectively, and are the leading order terms in established flames (Klein *et al.*, 2008). At $t/t_{sp} \approx 0.75$, P_2 is negligible, while D_2 is not, due to the large temperature gradients found at the ignitor centre. The magnitude of both P_2 and D_2 increases with time, and they eventually become leading order shortly after the spark has been switched off ($t/t_{sp} \approx 1.3$). After the thermal runaway occurring at $t/t_{sp} \approx 1.9$ for $u'/s_l^0 = 9$ and Realisation 1, the value of both P_2 and D_2 increases by an order of magnitude, before decreasing slowly as $T_{\max}$ decreases to $T_{\max} = 1$ long after the ignition. For the realisations 2 and 3, both terms decrease after the spark is switched off due to the failed ignition.

Figure 6 also presents the temporal evolution for the ratio $\Lambda = \max(|\langle P_2|_T\rangle|)/\max(|\langle D_2|_T\rangle|)$, where $\langle\cdot|_T\rangle$ denotes the conditional mean on temperature evaluated over the whole domain. The competition between the chemical heat release and thermal diffusion controls the flame behaviour, if $\Lambda \geqslant 1$, the hot gas kernel expands in size, if $\Lambda \leqslant 1$, the flame quenches. It can be observed that a marker of successful ignition is that $\Lambda > 1$ at $t = t_{sp}$, which would indicate that the ignition success is fully determined at $t = t_{sp}$. The value of $T_{\max}$ reached at $t = t_{sp}$ is not the only parameter governing this competition, as highlighted by the very different values of Λ reached at $t = t_{sp}$ for the three turbulent realisations of $u'/s_l^0 = 9$ although similar $T_{\max}$ values are observed on Fig. 5. The overall thermal diffusion D_2 variations thus appear to play a key part in determining the success or failure of an ignition event.

To study this effect, D_2 can be decomposed ($D_2 = D_{21} + D_{22}$) into its normal $D_{21} = \mathbf{N}\cdot\nabla(\lambda\mathbf{N}\cdot\nabla\hat{T})$ and tangential components $D_{22} = -\lambda|\nabla\hat{T}|\nabla\cdot\mathbf{N} = -2\lambda\kappa_m|\nabla\hat{T}|$, where $\mathbf{N} = -\nabla\hat{T}/|\nabla\hat{T}|$ is the local isotherms normal vector pointing towards the reactants, and $\kappa_m = 1/2\nabla\cdot\mathbf{N}$ is the local curvature of isotherms. This decomposition is shown for $u'/s_l^0 = 9$ and $\Gamma = \Gamma_{\text{MIE}}$ for all turbulent realisations in Fig. 6 at $t = 1.05t_{sp}$. The tangential diffusion contribution (D_{22}), which is directly proportional to the isotherms curvature, behaves similarly for all turbulent realisations and does not seem to significantly affect the ignition process. This is consistent with the fact that at such early times, the temperature isosurfaces curvature is driven principally by the thermal diffusion from the ignitor centre which deposits energy within the characteristic distance R_{sp}. However, the normal component (D_{21}) differs significantly depending on the turbulent realisations. This may be due to the local isotherm curvature as seen on the probability density function (PDF) of κ_m that is wider for realisations 2 and 3 than for the first one on the isotherm $T = 0.3$, indicating that κ_m can be locally much larger, even though the PDFs mean values are comparable. This curvature variation leads to significant local variations of D_{22} although its mean value remains mostly unaffected, but additionally local behaviours of $|\nabla\hat{T}|$ and D_{21} are also affected by the correlation between $|\nabla\hat{T}|$ and κ_m. This is reflected in the consistently larger magnitude of D_{21} for realisations 2 and 3 compared to realisation 1, which, in turns leads to a larger magnitude of negative thermal diffusion term (D_2). This indicates that the spatial fluctuations of curvature that are due to the local turbulent motions significantly affect the magnitude of D_2 through their influence on the normal contribution (D_{21}). Subsequently, the overall thermal diffusion can locally supersedes the chemical heat release rate, and lead to a misfire. This thus shows how the local randomness of turbulence affects the temper-

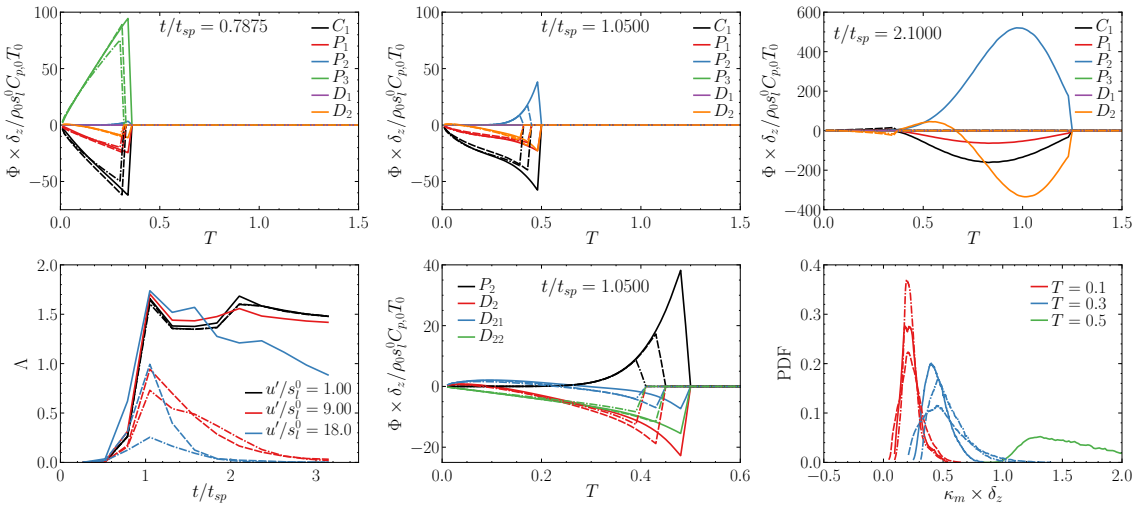

Figure 6: **(top)** Energy budget for $u'/s_l^0 = 9$ and $\Gamma = \Gamma_{\text{MIE}}$, **(bottom)** *(left)* Temporal evolution of Λ for different u'/s_l^0 and $\Gamma = \Gamma_{\text{MIE}}$ *(centre)* Normal (D_{21}) and tangential (D_{22}) components of D_2 for $u'/s_l^0 = 9$ and $\Gamma = \Gamma_{\text{MIE}}$ *(right)* Isotherms curvature for $u'/s_l^0 = 9$ and $\Gamma = \Gamma_{\text{MIE}}$ - ——— Real. 1, -·-·- Real. 2, - - - - Real. 3

ature distribution and ultimately controls the success or failure of a given ignition event, whilst everything else is kept constant (u'/s_l^0, l_t, Γ, R_{sp}, b_{sp}, etc.).

5 Conclusions

The minimum ignition energy (MIE) of a stoichiometric methane-air mixture in an homogeneous isotropic decaying turbulence has been numerically evaluated for a large range of initial turbulence intensities. A good qualitative agreement has been found with the experimental findings (Huang *et al.*, 2007 ; Shy *et al.*, 2010), with the prediction of a transition in the MIE between low to moderate and large turbulence intensities. However, there are discrepancies in the u'/s_l^0 dependence of the MIE between experimental and computational results. This lack of quantitative agreement can be attributed to the fact that in DNS all the energy is used to heat the fluid unlike the experiment. The fundamentally stochastic behaviour of the ignition has also been reproduced numerically by sparking three statistically identical realisations of turbulence (identical u'/s_l^0 and l_t) and measuring the probability of successful ignition. Furthermore, the energy distribution following its deposition was investigated and it was found that ignition was successful only if the maximum value of the chemical heat release to the thermal diffusion magnitude ratio was greater than unity at the end of the energy deposition. Finally, the stochastic behaviour of the ignition process was attributed to the key role of the spatial fluctuations of local isotherms curvature which in turns affect the normal component of diffusion and thus the overall thermal diffusion rate. Therefore a misfire follows if the magnitude of overall thermal diffusion rate supersedes the heat release rate.

Acknowledgments

The authors are grateful to the British Council, EPSRC and ARCHER for financial and computational support respectively.

References

Ballal, D.R. and Lefebvre, A.H. (1975), The influence of flow parameters on MIE and quenching distance, *Proc. Combust. Inst.*, Vol.15, pp.1473-1481

Batchelor, G.K. and Towsend, A.A. (1948), Decay of turbulence in final period, *Proc. Roy. Soc. Lond.* , Vol.A 194, pp.527-547

Bradley, D. and Lung, F.K.K. (1987), Spark ignition and the early stages of turbulent flame propagation, *Combust. Flame*, Vol.69, pp.71-83

Baum, M. and Poinsot, T. (1995), Effect of mean flow on premixed flame ignition, *Combust. Sci. Technol.*, Vol.106, pp.9-39

Espi, C.V. and Liñán A. (2001), Fast, non-diffusive ignition of a gaseous reacting mixture subject to a point energy source, *Combust. Theory Model.*, Vol.5, pp.485-498

Huang, H.H., Shy, S.S., Liu, C.C. and Yan, Y.Y. (2007), A transition on MIE for lean turbulent methane combustion in flamelet and distributed regimes, *Proc. Combust. Inst.*, Vol.31, pp.1401-1409

Klein, M., Chakraborty, N. and Cant, R.S. (2008), Effects of turbulence on self-sustained combustion in premixed flame kernels : A DNS study, *Flow. Turb. Combust.*, Vol.81, pp.583-607

Mastorakos, E. (2009), Ignition of turbulent non-premixed flames, *Prog. Energy Combust. Sci.*, Vol.35, pp.57-97

Mulla, I., Chakravarthy, S.R., Swaminathan, N., Balachandran, R. (2010), Evolution of flame-kernel in laser-induced spark ignited mixtures: A parametric study, *Combust. Flame*, Vol.157, pp.341-350

Patel, D. and Chakraborty, N. (2015), Effects of energy deposition characteristics on localised forced ignition of homogeneous mixtures, *Int. J. Spray Combust. Dyn.*, Vol.7, pp.151-174

Peters, N. (2000), Turbulent Combustion, 1^{st} ed., Cambridge University Press, Cambridge, UK

Shy, S.S., Liu, S.S. and Smith, W.T. (2010), Ignition transition in turbulent combustion, *Combust. Flame*, Vol.157, pp.341-350